DOI: 10.15480/882.9301

Eighth International Symposium on Marine Propulsors
smp'24, Berlin, Germany, March 2024

Gate Rudder System and Ship Design

Noriyuki Sasaki, Mehmet Atlar

Naval Architecture, Ocean and Marine Engineering (NAOME), University of Strathclyde, Glasgow, UK

ABSTRACT

The Gate Rudder System (GRS) is a new integrated propulsion system that combines steering and propulsion uniquely and unconventionally. This system's most distinctive application feature is that the existing rudder is removed from the original position, and two new rudder blades are placed either side of the propeller. As a result, the rudder, which is conventionally a resistance source, becomes a propulsion device that can generate thrust.

In addition to the above hydrodynamic advantage, the effect of the hydrodynamic side force generated on the gate rudder when the ship is sailing with a drift angle provides the hull with a high course stability and smaller yawing and rolling motion in wind and waves. This reduces the in-service resistance.

The advantages mentioned above and other unique features of the gate rudder system (GRS) suggest a rethinking of conventional hull form design and lead to new types of hull forms that may not have existed so far, as discussed in this paper.

Keywords

Gate Rudder, Energy Saving Device, Open type Ducted Propeller, Scale Effect of thrust deduction factor

1 INTRODUCTION

The rudder blades of a GRS can increase the pressure near the stern end of the hull due to their displacement effect (Sasaki et al., 2021; Sasaki & Atlar, 2019), while the propeller's action further affect this hydrodynamic phenomenon.

The pressure recovery at the ship stern caused by the above-mentioned effects will reduce the pressure drop due to the propeller action, the well-known phenomenon of thrust deduction. Consequently, the thrust deduction factor can be dramatically minimised.

Recent investigations with a GRS, including full-scale measurements, revealed that the model test-based thrust deduction factor obtained with this system showed a remarkable scale effect (Sasaki, 2023). This may suggest that the model test-based performance predictions will not present accurate gate rudder performance if this scale effect is not considered in the analysis procedures of the model tests.

Since the GRS' blades generate thrust and their displacement effects push the ship's stern end, the hull resistance at the propelled condition is significantly reduced. In contrast, the towing resistance of both configurations, i.e. the conventional rudder (CR) and the gate rudder (GR), is almost similar. Depending on the ship type, this reduction in hull resistance at the propelled condition can vary between 15% to over 30%. Since propeller thrust is proportional to the hull resistance, this reduction also manifests itself as the reduction in the propeller thrust, requiring less engine power demand if the propeller working condition is not so far from the original propeller.

This paper first reports on the above-described scale effect phenomena based on the numerical, experimental, and full-scale investigations conducted in the H2020 GATERS project (Atlar et al., 2023; Atlar, 2022). The study then investigates and discusses the effect of the hydrodynamic side force generated on the gate rudder blades when the ship is sailing with a drift angle and claims that the GRS provides the hull with significantly improved course stability and smaller yawing and rolling motion in wind and waves, resulting in better powering performance in-service.

The above-mentioned unique features of the GRS require a rethinking of conventional hull form design, which may lead to new types of hull forms that have not yet existed, as discussed in this paper for a 210k DWT bulk carrier example. The paper also explores further favourable applications of the GRS. First is the best solution to solve the conflict between the IMO's EEDI and Minimum Propulsive Power (MPP) in meeting these requirements

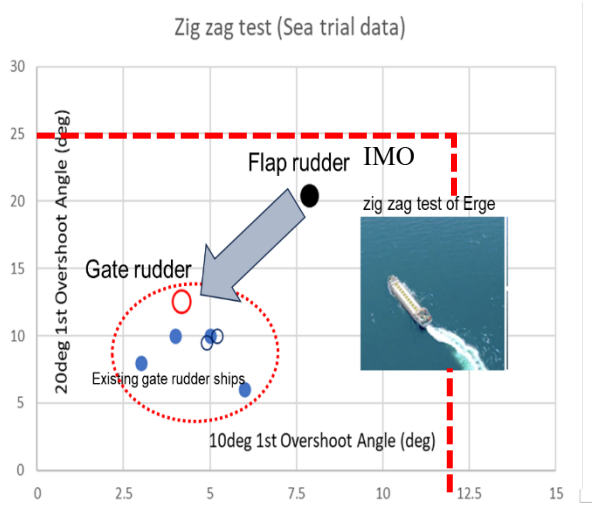

Figure 1a: Course keeping ability of MV ERGE: before & after GRS Retrofit

simultaneously for a 24k DWT bulk carrier case. The second and third complementary applications are associated with wind-assisted ships and silent propulsion, respectively.

Following the GATERS project's successful results, many business opportunities have been developed. Some purely use the GRS technology, but others combine the GRS with other ESDs. The authors are slightly concerned that the gate rudder technology has not been deeply investigated in terms of the interaction with other ESD(s). Finally, the authors report on the problems they have experienced with the model tests and CFD, which may confuse ship designers when applying the GRS technology and can prematurely stop the projects. At the same time, the GRS applications presented six excellent ships with this technology operating in service so far.

By utilising the characteristics of the GRS introduced in the following sections, it is possible to create a completely new ship that has never been seen.

Figure 1a compares the manoeuvrability of ships with GRS to those with a conventional rudder system (CRS). The figure shows that a ship's course stability can be significantly improved by equipping it with a GRS. For example, for the GATERS target vessel (MV ERGE) case, the tables with the CRS and GRS are presented in Figure1b. The criteria for the first overshoot angles for 10-degree and 20-degree steering (10OSA, 20OSA, are given in Equation (1) and (2).

$$10OSA : 5 + 0.50L/V = 12.03 \quad (1)$$

$$20OAS: = 25.00 \quad (2)$$

where L = ship length (m); V = ship speed (m/s); OAS = Overshoot Angle

Date : 23/1/2023, ERGE SEA TRIALS

HİDROTEKNİK NAUTICAL DESIGN & DEVELOPMENT

ZIGZAG 10/10 -STARBOARD

L/V	13.648	s	Criteria
First Overshoot Angle	9.7	°	5+0.5L/V =11.824
Second Overshoot Angle	11.1	°	17.5+0.75L/V =27.736
Initial Turning	21.4	s	
Yaw checking	20.1	s	
Reach	78.6	s	
Cycle time	150	s	
Start Speed	12.1	knots	

Date : 29/4/2023, ERGE SEA TRIALS

HİDROTEKNİK NAUTICAL DESIGN & DEVELOPMENT

ZIGZAG 10/10 -STARBOARD

L/V	14.06	s	Criteria
First Overshoot Angle	2.7	°	5+0.5L/V =12.03
Second Overshoot Angle	2.4	°	17.5+0.75L/V =18.04
Initial Turning	23.9	s	
Yaw checking	10.1	s	
Reach	59.3	s	
Cycle time	115.4	s	
Start Speed	11.75	knots	

Figure 1b: The example of the official record of zig zag (Insel & Saydam, 2023)

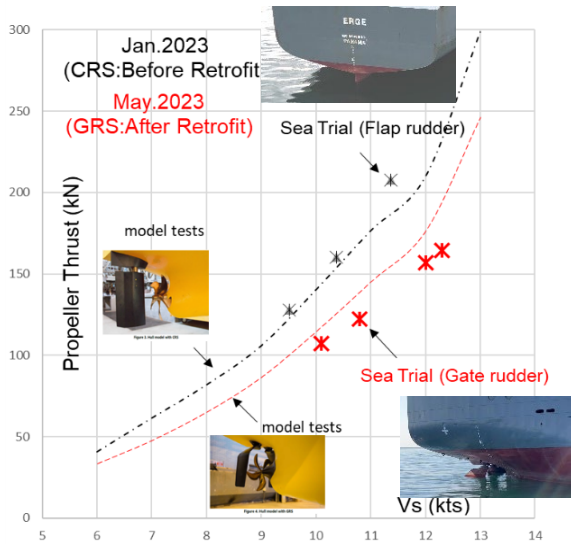

Figure 2: Significant reduction in hull resistance by gate rudder system (GRS) retrofit.

By taking a large bulk carrier as an example, the wave-making resistance of this type of hull form is relatively small, so there has been a search for an economical hull design by making it wider. However, the biggest barrier to this is the manoeuvrability, specifically the course-keeping ability. However, this obstacle can be removed by a GRS. Furthermore, considering the aft-end flow characteristics

of such vessels, the advantage of the GRS is also expected to increase.

Figure 2 compares the required propeller thrust at the same ship speed for the GATERS project's target ship MV ERGE, which was retrofitted with a GRS by replacing her conventional rudder system (CRS) on April 2023. In this figure, the comparative performance results are given based on the sea trials with the CRS in January 2023 and with the GRS in May 2023. Therefore, the accuracy of the data is much better than in other cases testing the same ship with two different rudder systems (Gurkan et al., 2023; Sasaki et al., 2017, 2018).

Figure 2 also includes the results of the model tests, which were conducted by CNR using a 7 m-long scaled model of MV ERGE. It is obvious that the reduction of the propeller thrust (resistance at the propelled condition) is not fully detected by the model tests compared to the full-scale data. The reduction of the resistance at 11kts (design speed) obtained by the GRS is 32% (sea trial) and 18% (model test), respectively.

Figure 2 was obtained from the measured torque of the official speed trial result submitted by Hidroteknik. According to the speed trial reports, the sea state of the CRS case is Beaufort 3 while the GRS case is Beaufort 2. The effect of the weather condition is estimated as 4% (0.15kts) for the mean values of double run. This implies that the CRS prediction by the model test is accurate.

This provide several performance advantages such as (1) fuel saving, (2) reduction of noise and vibration, (3) low wash, and (4) longer antifouling life, etc.

Another remarkable advantage of the GRS is the damping effect on the ship's motions at manoeuvring, including the operating conditions in wind and waves. The reduced ship motion seems to originate from the gate rudder's self-stabilising ability, which can reduce the drift angle during the yaw motion. Figure 3 to Figure 5 show the clear difference in drift angle of two rudder systems obtained from the zig-zag tests of Japanese container ships, Sakura and Shigenobu, during the joint sea trial (Atlar et al., 2023). The principal dimensions of these container ships are shown in Table 1.

Table 1: Dimensions of Japanese Container Ship

	Sakura	Shigenobu
Loa (m):	111.4	
B (m):	17.8	
d (m):	5.24	
Main Engine:	3309kW x 220rpm	
Rudder:	Flap Rudder	Gate Rudder
Delivery:	August 2016	December 2017

The smaller drift angle can contribute to safe steering, as shown in Figure 5. These three figures represent the ship trajectory obtained from the same zig-zag test. The ship with CRS (blue) shows a quick change in her heading angle compared with the ship with GRS (red). However, the ship with CRS is not able to avoid the collision due to her large drift angle. Because the IMO zig-zag test procedure requires the use of the information of her heading angle instead of her actual course, the GRS will require more length and time to change the rudder angle. Therefore, it is meaningful to discuss how we can compare the gate rudder's course-keeping ability when we consider this

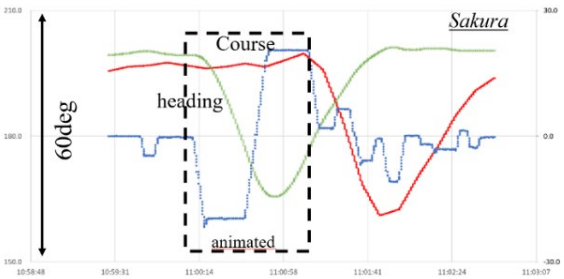

Figure 3: Relationship between the heading angle and the ship course for Sakura

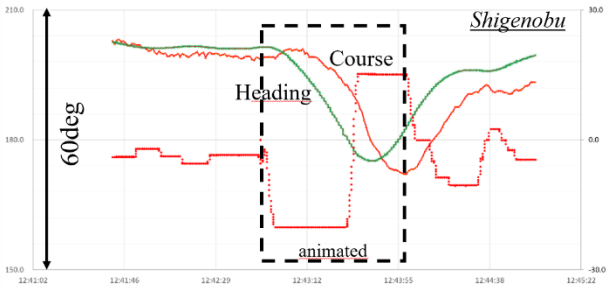

Figure 4: Relationship between the heading angle and the ship course for Shigenobu

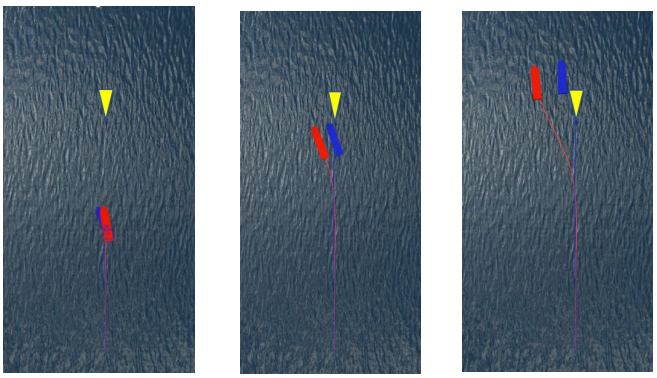

Figure 5: Difference of ship trajectory for CRS (blue) and GRS (red).

difference.

It is also important to know the impact on the zig-zag test when we use the ship course instead of her heading angle as an index of ship manoeuvring motion.

Taking those three remarkable advantages mentioned above, applying the gate rudder to twin-screw ships can be a good idea. There are two reasons for building costly twin-screw ships. One reason is that there is a limit to the thrust that a propeller can absorb, so it must be distributed

between two propellers. Another reason is safety and redundancy. Having two propulsion systems will ensure redundancy, including manoeuvrability, in the event of damage to the propulsion system. In the case of a gate rudder, the required thrust can be significantly reduced. The advantage is that basic manoeuvrability can be ensured by only one gate rudder and propeller.

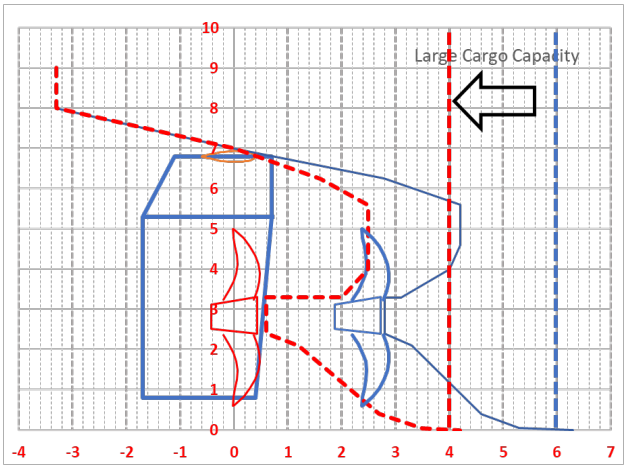

Figure 6: Modification of stern frame for large capacity.

The capability of the larger cargo capacity can be achieved by moving the engine room further aft, as shown in Figure 6. This is a simple solution for a vessel with a limited ship length when the ship owner needs to carry more cargo. This idea can increase the vessel's value when the ship designer has some restrictions, such as ship size according to the port requirements.

Since the propeller and rudder are not lined up in a GRS, the space where the rudder used to be is no longer needed, and that space can be used more effectively. Therefore, cargo space can be increased by moving the propeller and main engine room further aft of the ship. Also, if this is not necessary, a compact ship can be designed with a reduced overall length. This is valid if the length of the ship is restricted by the port.

2 PROPOSAL OF NEW SHIP USING GATE RUDDER SYSTEM

2.1 Ultra Beamy Bulk Carrier

Since ship design technology was considered to have reached enough maturity, shipyards have focused on reducing the cost of building ships. Large block construction with large block coefficient ships is probably the best example. On the other hand, ship construction costs are mostly determined at the initial stage when the ship's main features and propulsion system are determined, and it is difficult to reduce costs once the detailed design stage starts. The GRS has a large impact on its initial design strategy and requires sufficient time to be optimised. In particular, the installation position of the GRS will affect the subsequent stern arrangement as shown in Figure 6, so the overall optimisation should be pursued, including changes to the hull shape.

Table 2: Hull dimensions of a Newcastlemax-size bulk carrier

	Original (CRS)	GRS	Difference
Lpp (m):	295.2	270.0	-25.2m
Beam (m):	50.0	55.0	+5 m
Depth (m):	25.1		as original
draft (m):	16.1		as original
Deadweight:	21,000 ton		as original
Main Engine:	14,400 kW		as original
Rudder type:	Mariner	Gate R.	
Sea margin:	15%	8%	
Vs service:	13.3	13.7	

In order to study the effect of GRS on such a vessel of such size, we can consider a Newcastlemax design shown in Table 3 as an application to an ultra-beamy ship. The draft will be the same; the width of the ship will be increased by 10%, and the length will be shortened by 25.2m (8.5%). If a GRS is adopted for this ship type, it will perform almost the same as the original ship (with CRS) in calm water. However, a 6-7% improvement in fuel saving can be expected in actual voyages in addition to the power saving shown in Figure 7. This application aims to obtain better operating costs by fuel savings while the construction cost can be equivalent by reducing the hull steel weight. The powering procedure can be seen in Appendix 1.

The cost advantage of the reduced hull steel weight is assumed to be 2% of the total cost. The cost rise due to applying the GRS ranges between 4-5% of the machinery part, corresponding to 30-40% of the total cost. This means that the difference in the total cost is almost equivalent (CAPEX). We can obtain only the advantage of the GRS after her delivery as the lower operational cost (OPEX).

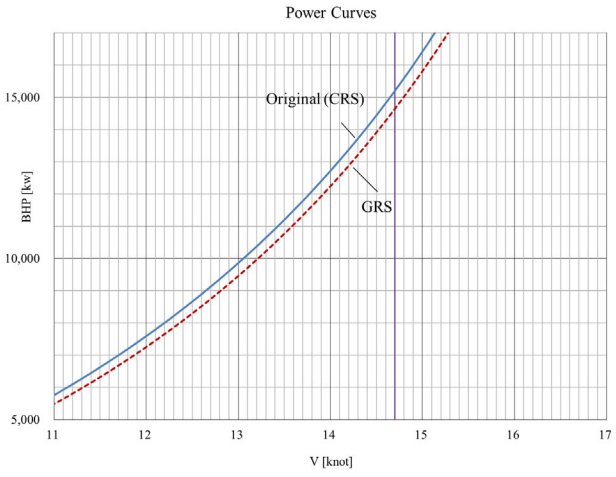

Figure 7: Estimated power curves for two B/C

2.2 Application to Ships suffering from the conflict between EEDI and MPP requirements

In 2011, the International Maritime Organization (IMO) established the Energy Efficiency Design Index (EEDI) as a goal-based technical standard to reduce the greenhouse gas (GHG) emissions generated by the shipping industry. Starting in January 2013, the initial two-year ("Phase-0") period required new ship designs to meet the reference level for their specific ship types. From then on, new ship designs are needed to become progressively more efficient in the next three "Phases", reaching a 30% reduction in CO2 emissions between 2025 and 2030 for applicable ship types.

Table 3: Dimensions of 24k DWT Bulk Carrier

Project name:	24k BC
DWT (ton):	24,600
EEDI (phase3):	5.1 (5.416)
MPP (level 1):	5220
Loa (m):	158.0
B (m):	25.0
D (m):	13.5
d design (m):	9.8
d scantling (m):	9.8
Service speed (kts):	12.5
Main Engine (kW):	3570
Fuel save by GRS:	26%

In addition to EEDI, there is a further IMO requirement called the Minimum Propulsion Power (MPP), addressing the safe manoeuvring of ships in adverse weather conditions. The critical requirements of the MPP are the propeller thrust and the maximum torque to satisfy the engine torque limitations.

As the EEDI requirements become more stringent through the implementation phases, it becomes a design challenge for large tankers and bulk carriers to meet the EEDI and MPP requirements simultaneously.

Within this context, the GRS significantly impacts meeting the regulations. To illustrate this positive impact, a 24k DWT Bulk Carrier with ship dimensions shown in Table 3 is selected. This recent project was completed successfully, and the associated class confirmed all procedures for Level 2.

Figure 8 shows the tank test result with a 4.5m model (with GRS) of the 24kBC conducted by the model basin, which also conducted the tests with the original ship (with CRS). The gate rudder shows the remarkable "Ducted Propeller Effect" on wake fraction, which can avoid excessive torque and increase the engine power higher than that of a Controllable Pitch Propeller (CPP), which has the same function by reducing the blade angle. The detailed logic will be explained in Appendix 2.

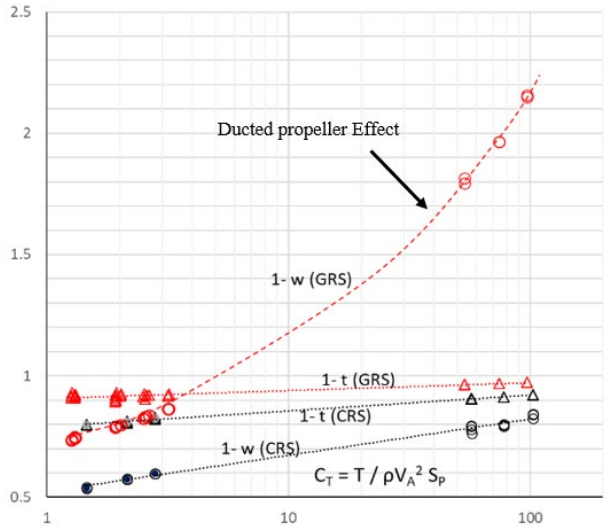

Figure 8: Propulsive coefficients obtained from model test with GRS for 24 kBC.

Figure 9 compares the required propeller thrust from IMO guideline Level 2 using the model test results. As shown in this figure, the GRS has a significant advantage in reducing the required propeller thrust. In Fig 9, “NK default” means the procedure NK recommends when the tank test data is unavailable. However, the authors doubt these default values because they are constant without considering the difference in propulsive coefficients for calm sea conditions.

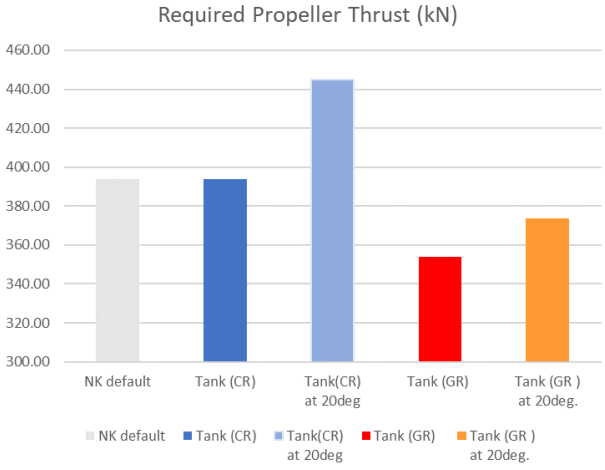

Figure 9: Required propeller thrust for CRS and GRS.

The impact of the rudder resistance at a 20 deg helm angle was also investigated in the model tests and included in Figure 9 and others for reference. The rudder resistance with the CRS during propelling conditions appears relatively high compared with the IMO guideline, which should be discussed for further improvement.

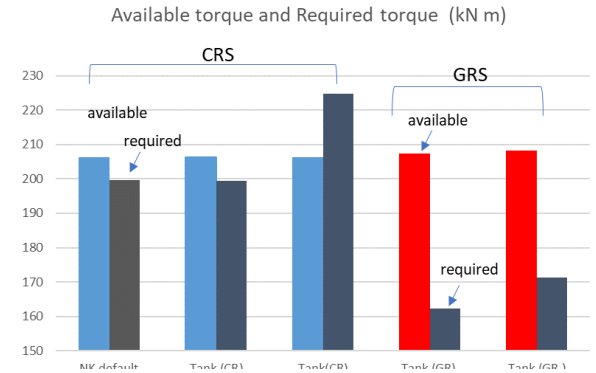

Figure 10: Required and available propeller torque.

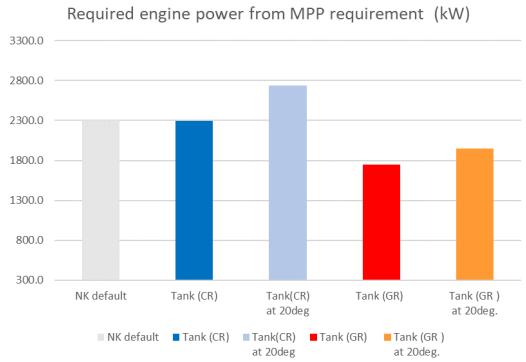

As stated at the beginning of this section, the key issues are the required propeller thrust and the maximum available torque to obtain the best performance. The higher advanced velocity in adverse conditions (at higher propeller loading conditions) will reduce the propeller torque and engine load.

Figure 10 shows a clear view of the massive advantage of the GRS in the safety margin, which is eight times the margin required for the CRS, i.e., a 3.5% (CRS) and 27.6% (GRS). Owing to this advantage, the required engine power

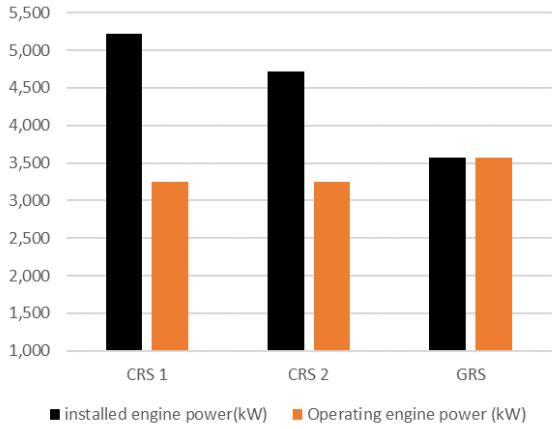

Figure 12: Installed engine and operating engine.

from MMP Level 2 differs largely, as shown in Figure 9. If we apply the same safety margin for both systems, the proper engine power is 3570kW (GRS) and 4722kW (CRS). Figure 12 shows the installed engine and operating engine for the different design cases listed in Table 4.

Table 4: Design alternatives.

	GRS	CRS 1	CRS 2
Rudder type	Gate Rudder	Conv. Rudder 1	Conv. Rudder 2
Propeller dia.	4.45m	4.7m	4.7m
Req. Tp (kN)	354	394	394
MPP (L1)	5220	5220	5220
EPL	---	EPL	EPL
MCR 1	3,570	5,220	4,722
MCR 2	3,570	3,250	3,250
Vs (75%MCR)	12.5	11.4	11.4
EEDI	5.1	5.1	5.1
MPP (L2 req)	1,743	---	2,306
MPP(L2 att.)	1,922	---	2,542
Cost (engine)	100	146	134

As shown in Figure 12, the conventional rudder system requires the installation of the engine with higher

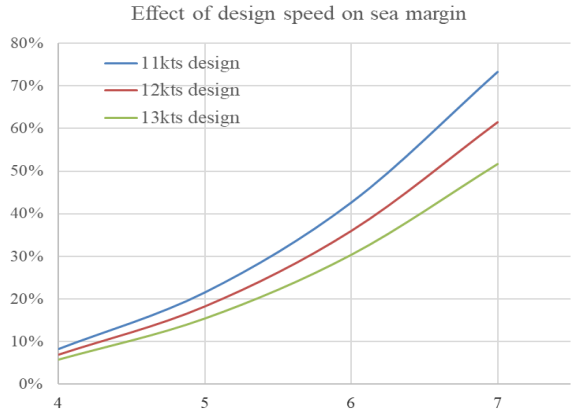

Figure 13: Effect of the design ship speed on sea margin.

propulsion power regardless of the application levels (Level 1 or Level 2), while the operating engine power is limited due to the requirement of EEDI Phase 3. We need to pay attention to cost and the design ship speed because the sea margin for the lower ship speed tends to increase considerably, as shown in Figure 13.

It is difficult to predict the difference in sea margin between the ships equipped with CRS and GRS because it strongly depends on the circumstances each ship will encounter after its delivery.

However, all the ship's voyage data with GRS shows excellent performance compared with the sister ships with GRS.

It seems there are multiple reasons already mentioned, such as the smaller drift angle, lower rudder resistance, duct propeller effect due to higher propeller loading and less ship motions etc. (Atlar, 2022; Bulten, 2023; Sasaki et al., 2018; Tacar et al., 2020; Turkmen et al., 2016).

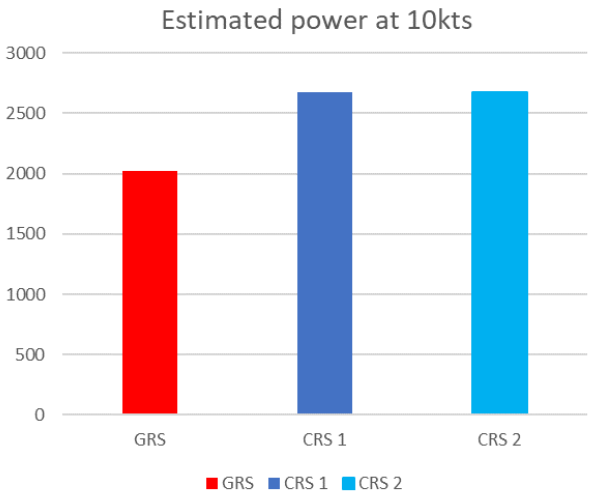

Regarding the sea margin (or power margin) calculation, the simplified method developed by Sasaki and given in Appendix 3 is used (Sasaki et al., 2009). The power saving (fuel saving) by the gate rudder will be 24% compared with the conventional rudder cases, as shown in Figure 14.

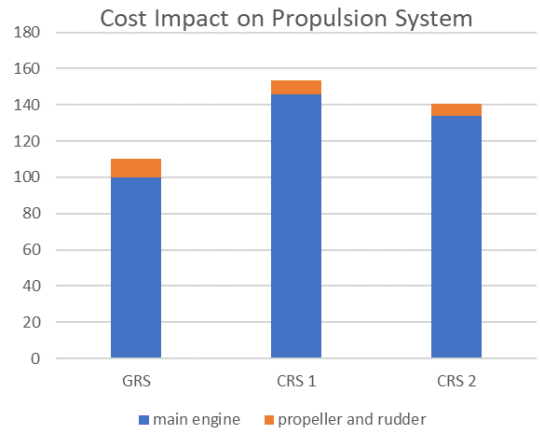

Figure 15: Cost impact of design alternatives (100%: slow steaming only)

The cost related to the main engine, such as the generators and boilers, has also increased. The cost of the gate rudder system is less than the cost of these machinery parts, as shown in Figure 15.

3 OTHER SPECIAL APPLICATIONS

3.1 WASP

We can apply the GRS to all kinds of ships without size, speed, and type limitations. However, some vessels show good chemistry with the GRS. The common ground is that those vessels operate under the strong effects of wind and waves. An excellent example of this type of vessel typically uses WASP (Wind-assisted ship propulsion) (Bulten, 2023).

The resistance produced by a conventional rudder operating at an angle relative to the vessel course will be vast. A 15-degree helm angle can increase the resistance by 30% of the hull resistance, which sacrifices the thrust obtained from the sails, as shown in Figure 16. The wind-assisted ship may sometimes require a sizeable bottom keel or a huge rudder to counterbalance this considerable drifting force and heeling moments. This means the potential energy saving expected by a WASP should take this handicap into account, as well as further maintenance tasks and design restrictions for their deck arrangement.

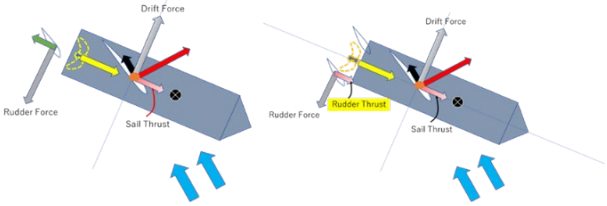

Figure 16: Force balance of WASP.

The GRS can effectively resist these drifting forces and counterbalance the heeling and yawing moments by its hydrodynamic lift based on the same mechanism as the sail on the deck. The difference is only the fluid density, i.e., the water density is 800 times the air density, which effectively operates the GRS as an "underwater sail." The reason we can call the GRS an underwater sail is explained in Appendix 4. An example of its application is shown in Appendix 5.

Figure 16 shows one typical case when the sole sail is located after the centre of rotation. The figure shows how we can compensate for the sail drifting force by the rudder, neglecting the hull hydrodynamic forces because those are the same for CRS and GRS ships.

3.2 Silent Ships

The next vessel types that the GRS application can complement are the vessels that require extremely low underwater radiated noise (URN), such as oceanographic research vessels and naval vessels that use active or passive sonars. The propeller-radiated noise is the most destructive phenomenon for a sound detection system.

The gate rudder significantly reduces the underwater radiated noise (URN), which was confirmed in the model and full scale (Atlar, 2022), Koksal et al., 2023). This advantage originated from the following three main reasons. i.e.,:

(1) Reduced thrust for the GRS compared to the CRS at the same ship speed,

(2) No presence of the rudder behind the propeller in the GRS

(3) Masking effect of URN by the GRS blades

Figure 17 shows the comparative full-scale URN measurements obtained from the joint sea trial of Japanese

Container Vessels (JCV: Sakura and Shigenobu) (Atlar, 2022). The difference in the URN level between the GRS and CRS is 10-15dB, which is significant.

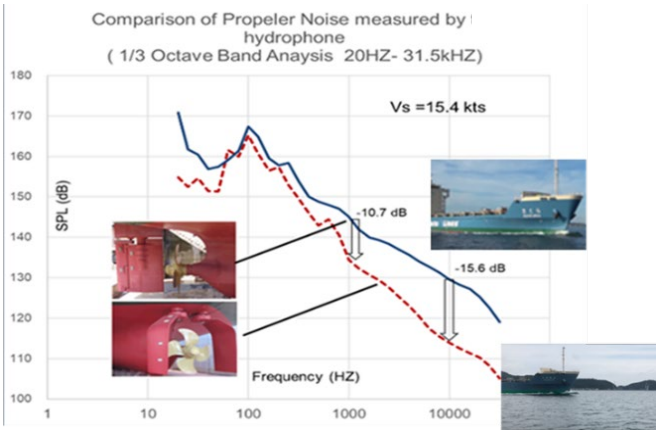

Figure 17: Difference of URN (CRS and GRS).

As stated above, the significant reduction in propeller thrust is the major contributor to this difference. Figure 18 shows the difference between JCV and MV ERGE propeller thrust, respectively, obtained from the model test and the full scale. Figure 18 also indicates that the existing model test procedure would not guarantee an accurate thrust measurement even with a large model, as experienced with the 11m model of Shigenobu and Sakura tested in the HSVA model basin.

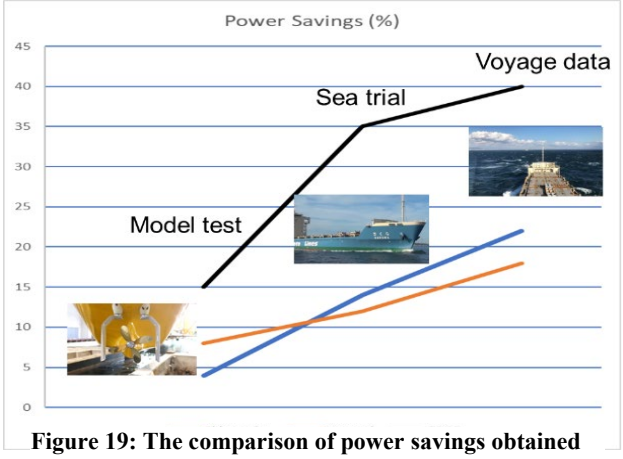

Figure 19: The comparison of power savings obtained from different sources.

Opposite Trend of the Model Test Results

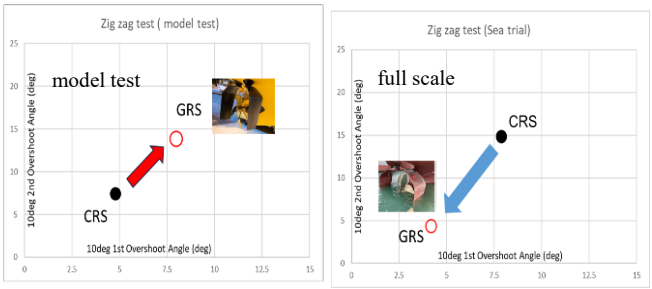

Figure 20: The comparison of zig-zag test conducted by the model and full-scale x: 10deg. 1st OSA, y: 10deg 2nd OSA

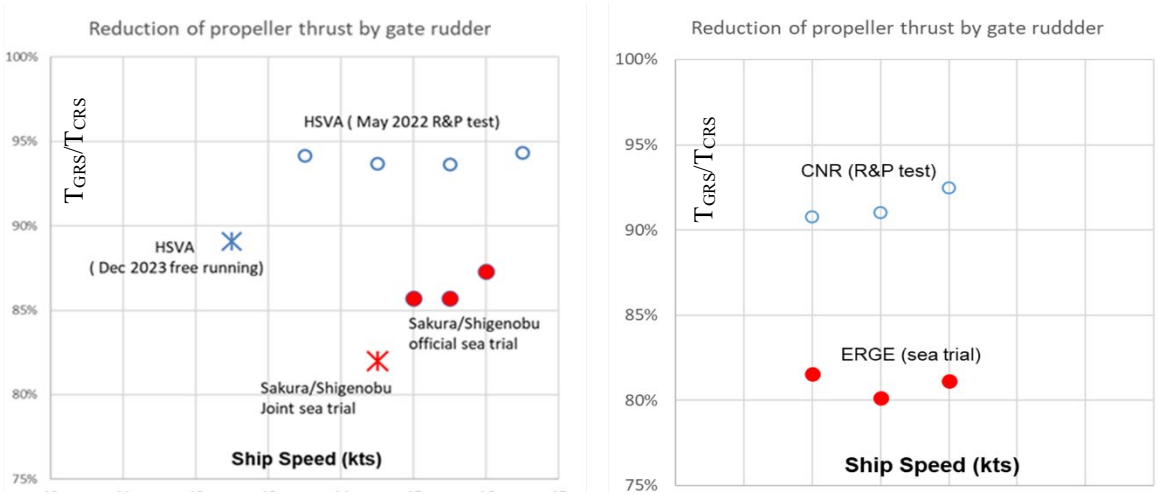

Figure 18: Reduction of propeller thrust by Gate Rudder of JCV (left) and Erge (right)

T_{GRS}: Prop. thrust of GRS, T_{CRS}: Prop. Thrust of CRS

4 A SPECIAL NOTE ON THE MODEL TESTS WITH GRS

The discrepancy shown in Figure 18 may affect all kinds of model tests with the GRS, not only the propulsion tests (Figure 19) but also other tank tests such as manoeuvring (Figure 20), sea keeping and cavitation tests.

One example of the above that was experienced in the GATERS project was the manoeuvring tests with MV ERGE, as illustrated in Figure 20, which compares the free-running zig-zag tests in the manoeuvring lake and sea trial. This figure implies that many tank tests with the GRS conducted by the model basins might suffer this opposite trend, requiring further investigation on the complex scale

effects which can appear even for ships with the CRS case as presented by Ueno (Ueno et al., 2014). Based on the model test results, it is easy to see that many commercial projects may be confused and terminated prematurely in the development stage.

Figure 19 shows the general trend of power savings obtained from model tests with a large model, sea trials and voyage data. It is obvious that some parts of the discrepancies are caused by the problem with the model test procedure, and weather conditions cause some of them.

5 CONCLUSIONS

The unique features of the gate rudder system (GRS) require a rethinking of conventional hull form design and lead to new types of hull forms that may not have existed so far. This paper introduced four unique applications, and the results can be summarised as follows:

(1) A large bulk carrier with 210k DWT was studied by adopting a shorter ship length and broader beam with the same deadweight. If a GRS is adopted for this ship, the vessel will have better fuel-saving performance (around 8%), while the construction cost can be equal by cancelling the cost rise of the GRS by saving from the hull steel weight.

(2) The GRS can be the best solution for the conflict between EEDI "Phase 3" and MPP requirements. The example of the application to a 24k DWT bulk carrier was studied, and this concluded that the initial cost (as the main part of CAPEX) could be reduced by 39% (CRS Level 1) and 28% (CRS Level 2), respectively. After the delivery, fuel saving (as the main part of OPEX) at 10kts is about 24%, based on the difference in their sea margins.

(3) The GRS can be highly complementary for ships with WASP and requiring silent propulsion. It can significantly improve their performances by effectively counterbalancing the wind yawing moment for the former and reducing the propeller thrust for both ship types.

(4) Regarding the model test and CFD-based tools, the prediction accuracy obtained from these design tools is currently insufficient for exploring the scale effect-related flow complexities. The discrepancies are significant, and the model test results can potentially stop the projects, while the existing GRS applications presented six excellent ships operating in service so far.

ACKNOWLEDGEMENTS

The Innovation Action project GATERS (ID:860337) is sponsored by the EC under the H2020 framework and conducted by its 18 partners as stated in GATERS et al. (2020) and the project website:

http://www.gatersproject.com/

REFERENCES

Atlar, M., Aktas, B., Gurkan, A., Sasaki, N., Sun, X., Korkut, E., & Felli, M. (2023). The GATERS Project – An innovative way of retrofitting ships for greener and safer operations. *Transportation Research Procedia*, *72*, 1958–1965. https://doi.org/10.1016/J.TRPRO.2023.11.676

Atlar. M. (2022). GATERS-Gate Rudder System as a Retrofit for the Next Generation Propulsion and Steering of Ships. *2nd Decarbonizing Shipping Forum*.

Bulten, N. (2023). Synergies of wind-propulsion and Gate-Rudder technology. *Wind Propulsion Conference 2023*.

Fujii, H., & Takahashi, T. (1975). Experimental Study on the Resistance Increase of a Large Full Ship in Regular Oblique Waves. *Journal of the Society of Naval Architects of Japan*, *1975*(137), 132–137. https://doi.org/10.2534/jjasnaoe1968.1975.132

GATERS (2020). Grant Agreement: GATERS-H2020-MG-2018-2019-2020 / H2020-MG-2019-TwoStages – No: 860337. The EC. May.

Gurkan, A. Y., Turkmen, S., Sasaki, N., Aktas, B., Koksal, C., & Atlar, M. (2023). Manoeuvrability Improvement Investigation of A Coastal Vessel Retrofitted with Gate Rudder System Using Computational and Experimental Methods. *7th International Conference on Advanced Model Measurement Technology for the Maritime Industry, AMT 2023*.

Insel, M., & Saydam, Z. (2023). Full-scale Measurement Uncertainty for Comparative Tests. *7th International Conference on Advanced Model Measurement Technology for the Maritime Industry, AMT 2023*.

Koksal, C., Gurkan, A. Y., Aktas, B., Turkmen, S., Zoet, P., Sasaki, N., & Atlar, M. (2023). Underwater Radiated Noise of Pre-and Post-Retrofit of Gate Rudder System During MV Erge Sea Trials. *7th International Conference on Advanced Model Measurement Technology for the Maritime Industry, AMT 2023*.

Maruo, H. (1963). Resistance in waves. *Researches on Sea-Keeping Qualities of Ships in Japan*, 67–102. https://cir.nii.ac.jp/crid/1570854175016250368

Sasaki, N. (2023). How can we explain 35-55% of the energy savings obtained from the target ship ERGE (keynote speech)? *INT-NAM'2023*, Istanbul

Sasaki, N., & Atlar, M. (2019). Scale Effect of Gate Rudder. *Sixth International Symposium on Marine Propulsors Smp'19, Rome, Italy, May 2019*.

Sasaki, N., Kuribayashi, S., Asaumi, N., Fukazawa, M., Nonaka, T., Turkmen, S., & Atlar, M. (2017). Measurements and Calculations of Gate Rudder Performance. *International Conference on Advanced*

Model Measurement Technology for the Maritime Industry, 358–388.

Sasaki, N., Kuribayashi, S., & Atlar, M. (2018). Gate Rudder. *Third International Naval Architecture and Maritime Symposium-INTNAM*, 89–108.

Sasaki, N., Kuribayashi, S., Bulten, N., & Yazawa, M. (2021). Joint Sea Trial of Ships with Gate Rudder and Conventional Rudder. *RINA Full Scale Ship Performance Online Conference*.

Sasaki, N., Ohmatsu, S., Matsubara, T., & Yoshida, T. (2009). Practical Calculation Method of Sea Margin. *JASNAOE*, *8*, 399–402.

Tacar, Z., Sasaki, N., Atlar, M., & Korkut, E. (2020). An investigation into effects of Gate Rudder® system on ship performance as a novel energy-saving and manoeuvring device. *Ocean Engineering*, *218*, 108250. https://doi.org/10.1016/j.oceaneng.2020.108250

Turkmen, S., Sasaki, N., Atlar, M., Miles, A., & Takeda, T. (2016). The Gate Rudder Application to Improve Poor Course Keeping Ability of Ships. *A. Yücel Odabaşı Colloquium Series - 2nd International Meeting on Recent Advances in Prediction Techniques for Safe Manoeuvring of Ships and Submarines*.

Ueno, M., Tsukada, Y., & Kitagawa, Y. (2014). Rudder effectiveness correction for scale model ship testing. *Ocean Engineering*, *92*, 267–284. https://doi.org/https://doi.org/10.1016/j.oceaneng.2014.10.006

APPENDIX 1

The powering method used in Figure 7 is briefly described in this Appendix. The method estimates the resistance and propulsive efficiency based on the hull dimensions and some geometrical parameters such as CPf, CPA, etc.

Regarding the total resistance (R) calculations, the following form factor (K) method is used.

$$R = (1 + K)R_F + R_W \qquad \text{(A1.1)}$$

Here, R_F and R_W is frictional resistance and wave resistance, respectively.

In the procedure, R_W is calculated by the following the formula:

$$RW = f(BF1) * 1/2\,\rho V s^2 * S\ for\ Cpf > 0.75$$
$$RW = f(BF2) * 1/2\,\rho V s^2 * S\ for\ Cpf < 0.75$$
$$BF1 = Cm * L/B * (1 - Cpf)/2$$
$$BF2 = B/L\ \ 1/(1 - Cpf) \qquad \text{(A1.2)}$$

Here, we will explain the frame line factor, one of this system's features. The validation was made based on the form factor (K) of various hull forms carried out at the National Maritime Institute over the past 30 years using the hull form parameter proposed by Taniguchi et al.

Here, it is known that the hull form that gives the smallest K for p is a hull form without eddies whose streamlines follow geodesics. By introducing the frame line factor (FLF), the difference in stern shape can be represented instead of the real geometry, as shown in the following Equation (A1).

$$K = KMOM + FLF * KVMAX \qquad \text{(A1.3)}$$

$$KMOM = 2.25 * p \qquad \text{(A1.4)}$$

Where KMOM means the K values corresponding to the hull shape with only momentum loss (without vorticities) and corresponds to, for example, a buttock flow hull type or parabolic stern shape.

KVMAX is the maximum increment (0.2) of K due to the longitudinal vortex generated by twisting the streamline by the frame line. Of course, the maximum has no physical meaning, but it was found that, when considering a practical hull form, it is not so reckless to set this to 0.2. The frame line factor (FLF) is a coefficient representing the strength of longitudinal vortices and takes a value from 0 to 1, and when FLF=1, the increment of K takes the maximum value KVMAX.

Although the frame line is a secondary hull shape coefficient for wave resistance, it is an important coefficient for K. In particular, the stern frame line of a blunt ship has a more important function than the main feature, so its selection must be carried out with multifaceted considerations such as vibration, manoeuvrability etc., at the basic planning stage.

To accurately determine the self-propulsion factor without any tank test or CFD calculation, understanding their physical meanings is essential and summarised as follows.

Because the hull shape is already optimised by the tank test and CFD study using a long period, the simple parameters can be used to within a few per cent based on certain hull form details and shape parameters. It seems possible to estimate the gate rudder case with enough accuracy.

The wake fraction w is divided into the hull and rudder components and is expressed as follows.

$$w = w_H + w_R \qquad \text{(A1.5)}$$

Here, the hull wake fraction w_H is divided into the viscosity w_{HV} and the hull potential component w_{HP}.

$$w_H = w_{HV} + w_{HP} \qquad \text{(A1.6)}$$

w_{HV} was a function of stern fullness parameter p, using the Cpa curve and propeller diameter ship stern draft ratio D_p/dA and K values, which were obtained from the resistance prediction part.

w_{HP} is the potential wake of the hull and w_R is also the potential wake generated by the rudder in front of it (rudder displacement effect). The values for the standard propeller diameter (set according to the ship type) are determined as follows.

$$w_{HV} = C1 * p + C2 * \Delta K \quad \text{(A1.7)}$$

where, $\Delta K = Kvmax * (ELF - 0.5)$

$$w_{HP} = 0.6/(S_x + 0.6)^3 \quad \text{(A1.8)}$$

Here, S_x is a numerical value representing the distance between the propeller and the hull. It is the value obtained by dividing the integral value of the horizontal distance from the 70% radius position of the propeller to the hull surface by the propeller diameter.

$$S_x = \int S_x(\theta)d\theta \ / \ 2\pi Dp \ (0 \leqq \theta \leqq 2\pi) \quad \text{(A1.9)}$$

In this system, S_x is approximated using the following formula so that calculation is possible even in the initial design where diagram information cannot be used.

$$1/S_x = 0.6/\ (p + 0.6\ )1.35 + 0.3 \quad \text{(A1.10)}$$

Next, the potential wake fraction w_R due to the rudder is determined by the following formula (Sasaki et al., 2021).

$$w_R = A1\ (\ 1 + g * ux\ ) * (A2)/(A3)^2 \quad \text{(A1.11)}$$

$$g = 1 + A3\ /\ \{\ 1 + (A3)^2\ \}^{0.5} \quad \text{(A1.12)}$$

$$A1 = 0.35 + 0.1 * A2 \quad \text{(A1.13)}$$

$$A2 = t_{max}/D_p \quad \text{(A1.14)}$$

$$A3 = dL/0.5D_p \quad \text{(A1.15)}$$

Here, ux is the wake coefficient of the propeller surface, dL is the distance between the propeller and the rudder, t_{max}/D_p is the ratio of the rudder thickness t_{max} at the shaft center height to the propeller diameter, and in the program, tmax is assumed 20% of rudder cord length CR at the shaft centre height.

Finally, the thrust reduction rate t is divided into the hull and rudder and calculated using the following formula (Sasaki, 2023).

$$t = t_H + t_R \quad \text{(A1.16)}$$

Furthermore, the thrust reduction rate t_H of the hull can be decomposed as follows.

$$t_H = t_{HP} + t_{HF} \quad \text{(A1.17)}$$

Here, t_{HP} and t_{HF} are the increment of pressure resistance and the increment of frictional resistance generated in the hull, respectively, and t_{HP} is theoretically the same as the potential wake w_{HP} of the hull, and frictional resistance is considered to be proportional to the thrust of the propeller is calculated using the following formula.

$$t_{HP} = w_{HP} = 0.6/(S_x + 0.6)^3 \quad \text{(A1.18)}$$

$$t_{HF} = 0.095 \quad \text{(A1.19)}$$

The thrust reduction rate due to the rudder is only affected by the rudder part that is in the wake of the propeller, so it is estimated using the following Equation. Here CR is the chord length of the rudder.

$$tR = (C3 + C4 * Tmax/CR) * CR * Dp\ /\ Ld \quad \text{(A1.20)}$$

APPENDIX 2

This Appendix shows the advantage of gate rudder for the safety manoeuvre at 2kts under extreme overload conditions.

The most important information is the engine torque limitations. Due to this limitation, the conventional propeller rudder system may not obtain enough power and this is not a simple evaluation by the propulsive efficiency. In the 24BC case introduced in this paper, we can compare the performance using Figure 6. According to the NK classification rules, added resistance can be calculated as follows:

$$R_a = R_{aw} + R_{aa} + R_{ar} \quad (A2.1)$$

In reality, these components are not the same for the CRS and GRS. The resistance of GRS is much smaller than that of CRS; however, we can follow the classification procedure.

If we start from the same resistance for the CRS and GRS, the required propeller thrust can be calculated using the thrust deduction factor.

Then, we are ready to start calculating the propeller's working condition using the given propeller's open water characteristics.

The results are as follows:

Table A2.1: Minimum power assessment based on NK rule

	CRS	GRS
Calm water resistance (kN)	8.15	8.15
Added rudder resistance (kN)	11.44	11.44
Added resistance by wind (kN)	86.99	86.99
Added resistance by waves(kN)	248.00	248.00
Total added resistance	354.58	354.58
Required propeller thrust	394.57	373.16
Load factor (KT/ J**2)	27.057	6.764
Advance coefficient	0.099	0.200
Propeller revolution	103.37	111.19
Torque coefficient	0.0261	0.0281
Required brake power	2036	1936
Required torque	187.85	166.28
Available brake power	1960	2263
Torque on load diagram	180.87	166.28
PB req < PB av	NG	OK
PBreq/PBav	103.9%	85.6 %

As shown in Table A2.1, a very important issue is the lower propeller working condition of GRS. This makes a larger safety margin for the available power (about 18% better than CRS).

The lower propeller working condition can be achieved by lowering the propeller pitch. Therefore, the CPP has the same advantage as the gate rudder.

APPENDIX 3
Simplified Calculation method performance in wind and waves

Added Wave Resistance Correction

This simple prediction method is entirely based on two theories except small new ideas. One is the Fujii-Takahashi method (Fujii & Takahashi, 1975), which predicts added wave resistance by reflection waves from a bow. Another one is the Maruo theory (Maruo, 1963), which predicts added wave resistance due to ship motion.

The differences between the present method and these theories are as follows;

(1) Added resistance due to ship motion is relatively small compared with the component due to the wave diffraction/reflection. Therefore, this resistance can be considered a function of ship length and wave height to simplify the calculation.

(2) Added resistance due to the diffracting/reflecting waves is assumed to be the dominant component for wave correction, and several assumptions are made to simplify the calculations as follows;

$$Raw = C_1 \times \frac{1}{2}\rho g(1 + C_2 {Fn_B}^{0.8}) \times \zeta a^2 \times B \times Bfcp \quad (1)Raw = C_1 \times \frac{1}{2}\rho g(1 + C_2 {Fn_B}^{0.8}) \times \zeta a^2 \times B \times Bfcp \quad (1) \tag{A3.1}$$

where, Raw is the added wave resistance of regular wave with height ζa. ρ and g is the density of water and gravity acceleration, respectively. B is a beam of a ship, and the most important factor, $Bfcp$, is the simplified bluntness factor obtained from the ship's principal dimensions instead of a water line geometry, which is required by the original theory. $Bfcp$ can be obtained by the next Equation assuming a rectangular Cw curve for a fore part. If the Cw value is not available, Cp value for a fore part can be used.

$$Bfcp = \frac{1}{1 + [2 \times (1 - Cpf) \times Lpp/B)]^2} \tag{A3.2}$$

(3) The effect of ship speed Vs can be regarded as an effect of Froude number based on a ship beam (Fn_B) instead of ship length (Fn) because the added wave resistance originates from the bow part. Therefore, the added wave resistance is not the function of Froude number based on ship length.

$$Fn_B = Vs/(gB)^{0.5} \tag{A3.3}$$

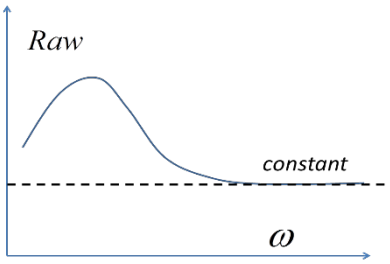

Figure A3.1: Assumption of constant Raw **for** ω

(5) The most efficient part of the present method will be the next Equation;

$$\overline{R_{AW}} = 1/2 \cdot R_{AW} \tag{A3.4}$$

This Equation was derived based on the following assumptions:

-Assumption 1:
Associated wave spectrum can be accepted as the Pierson-Moskowitz type given by the ISSC.

-Assumption 2:
Raw is constant and independent from wave frequency ω for the range of concerned wavelengths, as shown in Figure A3.1

Wind Resistance

Wind resistance is the most critical part of sea trial analysis because it has a high proportion of added resistance in sea trials conducted in ideal, calm weather conditions.

The following formula can represent the wind resistance.

$$R_{WIND} = C_0 \kappa(\phi) \rho_a V_{WIND}^2 A_F \tag{A3.5}$$

Here C_0 is the wind resistance coefficient for the headwinds, and $\kappa(\varphi)$ represents the effect of wind direction φ. These data can be estimated by several databases such as Fujiwara, Isherwood, Yamano etc., and shipyards may have their procedures. The present method utilises the Fujiwara method, which was developed based on the National Maritime Research Institute database.

Propulsive Efficiency

The differences between propulsive efficiency in the actual sea trial conditions and calm water predicted by towing tank tests can be divided into two categories:

The first one is propeller efficiency, which is a function of the propeller loading factor C_T represented by the following definition:

$$C_T = 8T/(\rho {V_A}^2 {D_P}^2) \qquad \text{(A3.6)}$$

Here, T, V_A and D_P is propeller thrust, advanced speed and diameter, respectively. According to momentum theory, propeller efficiency, the ratio of the propeller efficiency for the calm water and sea trial conditions, can be estimated by following Equation (A.7) without propeller characteristics.

$$\eta_o{}'/\eta_o = (1 + (1 + C_T)^{0.5})/(+(1{C_T}')^{0.5}) \qquad \text{(A3.7)}$$

Here, the prime (`) denotes the values related to the actual sea condition.

This approach is simple and accurate, as shown in Figure A 3.2, where the propeller efficiency is represented by an ideal efficiency function in the following Equation.

$$\eta_{o_{ideal}} = \frac{2}{1 + (1 + C_T)^{0.5}} \qquad \text{(A3.8)}$$

In Figure A3.2, the ordinate, "Experiments (MAU)", indicates the open water propeller efficiency of the MAU series from pitch ratio (H/D) 0.7 to 1.1 for all the propeller blade area ratios. Because we want to know the propeller efficiency change rather than the propeller efficiency, Equation (A3.7) is satisfactory.

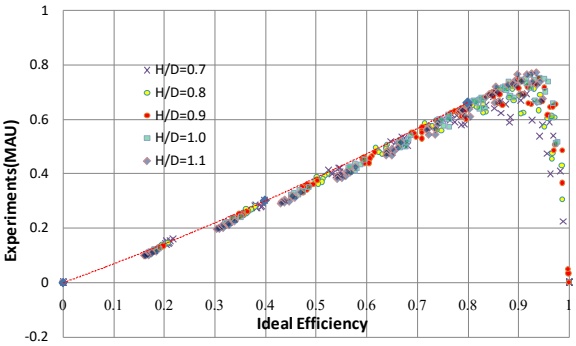

Figure A3.2: Relationship between experimental propeller efficiency and idea efficiency

The second category is a change of propulsive coefficients such as the wake fraction, w, thrust deduction fraction, t and relative-rotative efficiency η_R. It is generally recognised that the propulsive coefficients obtained from the model tests have scale effects. The most remarkable coefficient is the wake fraction w. The other two coefficients also have scale effects; however, these effects have been disregarded because the change is very small compared with the wake fraction. The general tendency of the wake fraction of the model scale is summarised as follows:

(1) Wake fraction w will decrease with ship speed
(2) Wake fraction w will decrease with thrust loading

The tendency can be explained by the effect of the Reynolds number and the change of the boundary layer thickness due to propeller suction, respectively. The change of wake fraction due to propeller loading is very large at the model scale, while the effect will diminish at full scale because the boundary layer of the full-scale ship is thin and propeller loading is weaker.

Therefore, the propulsive coefficients obtained from higher loading propeller and ship models to simulate actual sea conditions are not real, and the conventional model ship correlation for wake can only be used for calm sea conditions. This means that the change of propulsive coefficients due to propeller loading variation is very complicated, and further investigation is needed. The present method assumes that the propulsive coefficients will not change by variation in the propeller loadings, as in other sea trial analysis methods.

APPENDIX 4

We call the gate rudder " underwater sail" because the gate rudder can generate thrust, whilst the conventional rudder behind the propeller is not able to produce the thrust. This difference can be explained by the wing theory using the definition of lift and drag. The lift is a normal force to the flow direction ideally (2 dimensional) and the drag is a parallel force to the flow direction. In reality (3 dimensional), the lift force direction is inclined by the vortex system, and this effect generates so-called induced drag, as shown FigureA4.1

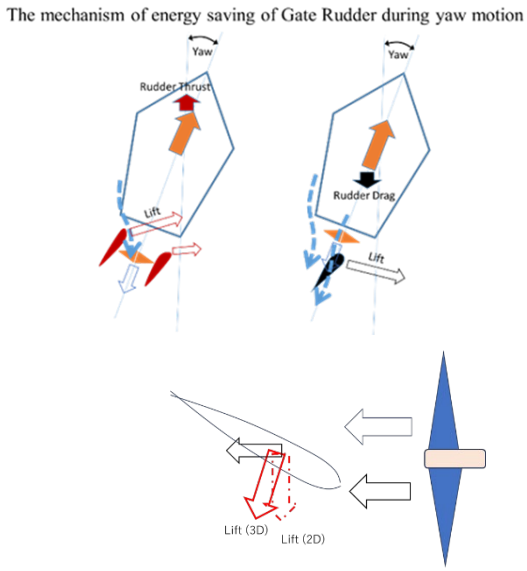

Figure A4.1: Importance of the flow direction to the resistance of the rudder

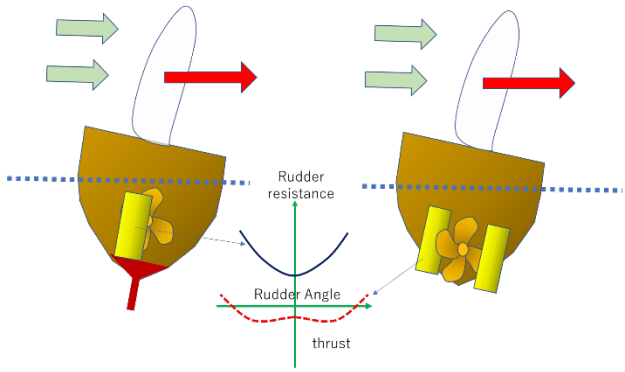

Figure A4.2: The difference of rudder resistance in the healing motion of WASP

The wind-assisted propulsion to prepare for the IMO's ever-stricter requirements, such as EEDI and EEXI, has been considered among European ship owners. However, wind force could generate a large drifting force and heeling force on the ship; consequently, we need a large helm to keep the ship course and avoid so-called leeway.

Because the flow direction for the conventional rudder behind the propeller is always deflected by the propeller (parallel to the ship's centre line), the conventional rudder generates only resistance, and the total hull resistance will be much amplified by ship motions such as yawing, rolling and healing.

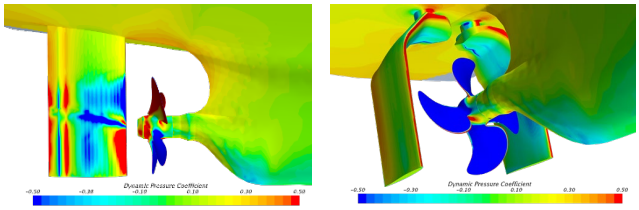

Figure A4.3: Pressure distribution on the rudders, left: CR, right: GR

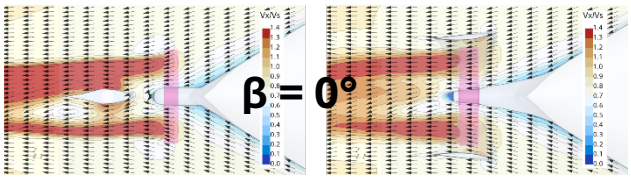

Here, we will add the CFD calculation data with drift angle

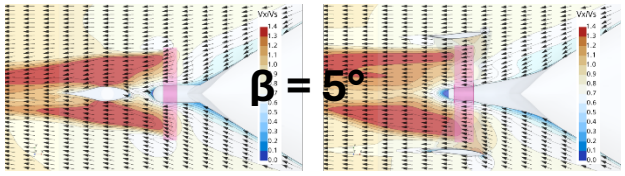

Figure A4.4: Vx/Vs distribution and the vector field around the rudders in self propulsion condition.

The resistance produced by the conventional rudder is huge. It quickly goes up 30% of ship resistance by only 15-degree steering and easily kills the valuable thrust obtained from the sail on the deck. Sometimes, the wind-assisted ship needs to be equipped with a large bottom keel to resist this large drifting force and heeling force. This means that energy-saving figures for sail-assisted ships should take this handicap into account in addition to the additional maintenance tasks and design restrictions for their deck arrangement.

The gate rudder can compensate this drifting force and heeling force by the lift force produced by the gate rudder based on the same mechanism as the sail on the deck. The difference is only fluid density, i.e. water is 800 times larger than air, which guarantees very effective under water sails.

APPENDIX 5

This Appendix presents an eexample of the GRS application to WASP.

The most important advantage of GS is the extremely small rudder resistance at the high rudder angle of more than 5 deg.

Case 1 Newcastlemax vessel:

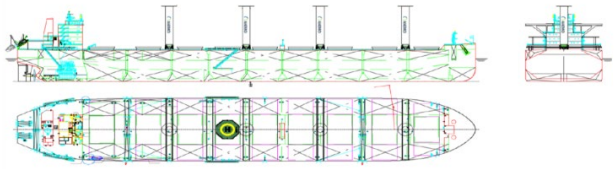

Figure A5.1: Proposed Arrangement for the Newcastlemax

Evaluation is made based on the following assumptions:

Table A5.1: Newcastle Max case assumptions

Target Ship:	Newcastle Max
Lpp*B*D*d:	294.0 * 50.0 * 18.00 * 16.1
Ship Speed :	14 kts
Equipped Rotor Area :	4 * 175 m**2
Ship Condition:	Design draft (16.1m)
M/E:	10139 kW at 14kts
Propeller Diameter:	9.0 m (Conventional Rudder)
	8.2m (Gate Rudder)
Wind condition	BF5
Wind Velocity, Direction	8.9m/sec, 90deg(S)
Rotor Power	173 kW

Table A5.2: Potential savings for the combined system.

Case	Sail thrust	Sail + Rudder	Power	FO save
CRS	0	0	10139 kW	-
WASP	500 kN	222 kN	8693 kW	14%
WASP+ GRS	500 kN	425 kN	6625 kW	35% + 8%

Case 2 CFD study by Wartsila:

Bulten (2023) demonstrated the advantage of GRS in his paper in his recent study claiming based on the following points:

(1) The known side forces from wind propulsion can, therefore, be better controlled with the Gate-Rudder.

(2) The Gate-Rudder generates a constant side force, which brings a clear synergy with wind-propulsion concepts.

Figure A5.2 shows the pressure distribution on the Gate-Rudder blades from two different viewing directions. In this condition, the rudders are in straight-ahead condition (0° steering) and only vessel leeway is applied in the simulations.

When looking at the inner side of the starboard rudder blade, the low-pressure region increases with larger leeway (drift) angles. This is in line with the theoretical concept. However, a second effect can be observed at the port-side rudder blade, where a larger low-pressure region at the shoulder-part section can be seen. This low pressure indicates a change in the angle of attack to the shoulder section.

The main flow is obstructed by the hull geometry, or in other words, the gate rudder is located in the shadow of the vessel. Reduction of the axial flow component in combination with the remaining radial component results in a change in the angle of attack and, therefore a different pressure distribution. The consequence of the two above-described phenomena results in a positive thrust force in the vessel's axial direction.

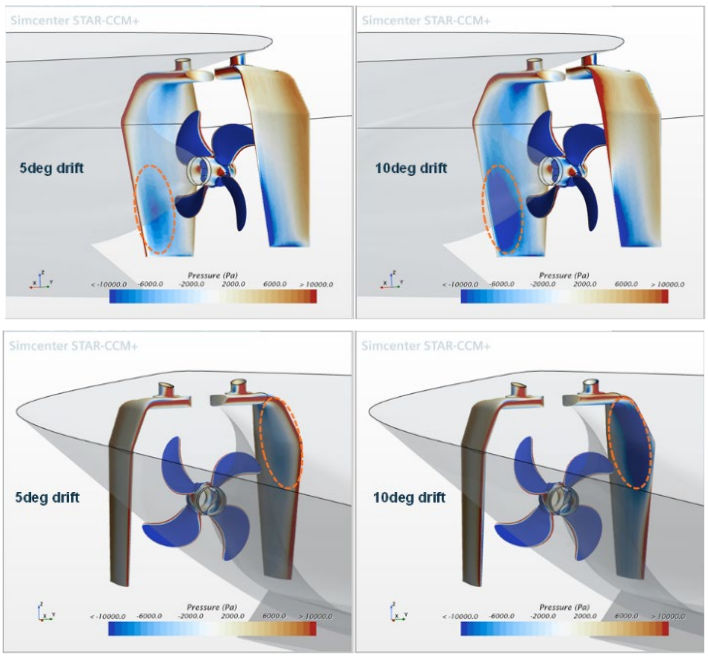

Figure A5.2: Pressure distribution on the gate rudder left: 5deg drift, right: 10deg drift.